Spin-Squeezing of ^{87}Rb via Optical Measurement

by

Adele Ann Schwab

Submitted to the Department of Physics
in partial fulfillment of the requirements for the degree of

Bachelor of Science in Physics

at the

MASSACHUSETTS INSTITUTE OF TECHNOLOGY

June 2008

Author .....
Department of Physics
May 12, 2008

Certified by .....
Vladan Vuletić
Lester Wolfe Associate Professor of Physics
Thesis Supervisor

Accepted by .....
David E. Pritchard
Thesis Coordinator

Spin-Squeezing of ^{87}Rb via Optical Measurement

by

Adele Ann Schwab

Submitted to the Department of Physics
on May 12, 2008, in partial fulfillment of the
requirements for the degree of
Bachelor of Science in Physics

Abstract

This project aims to reduce measurement uncertainty in atomic clocks by squeezing the collective spin of atoms. Spin-squeezing reduces noise below the standard quantum limit where precision scales as $1/\sqrt{N}$, allowing us to instead approach the Heisenberg limit where it scales as $1/N$. We report spin-squeezing of the $(F = 2, m_F = 0) \rightarrow (F = 1, m_F = 0)$ hyperfine transition of the $5S_{1/2}$ level of ^{87}Rb. We also demonstrate a viable setup for the spin-squeezing of the magnetically trappable $(F = 2, m_F = 1) \rightarrow (F = 1, m_F = -1)$ transition, which could potentially be used as a compact frequency standard. This thesis provides a brief theoretical background of spin-squeezing and a summary of the project in its current state.

Thesis Supervisor: Vladan Vuletić
Title: Lester Wolfe Associate Professor of Physics

To my birds, Boris and Ginger.

Acknowledgments

Firstly, I was very fortunate to work simultaneously with two splendid graduate students, Ian Leroux and Monika Schleier-Smith. I want to thank Ian for many long discussions and for his patience with numerous intuitive explanations of the physics and engineering behind the experiment. I also want to thank Monika for the many physical explanations and mathematical derivations she explained to me, and for her admirable attention to detail. Both of their upbeat spirits help make my work in the lab fun!

I would also very much like to thank my advisor, Vladan Vuletic, for his wonderful insight and physical intuition, as well as for his constant involvement in the status of the experiment.

In addition, I would like to thank Matthias Scholz for his many useful comments concerning this paper.

I would like to thank my parents for all their encouragement and emotional support; and particularly my mother, for never allowing me to feel afraid to be a woman in science.

And now that it's almost over, I should also thank the kids of senior haus and elsewhere for keeping me company these past four years, while continually reminding me to follow my passions and stay excited about life.

Adele A. Schwab

Contents

List of Figures

List of Tables

Chapter 1

Introduction

Physicists are constantly striving to push the frontiers of measurement precision to finer and finer scales. Measurement precision is extremely important to making new observations about the world. The speed limit of light was not well understood until Michelson and Morley invented their precise interferometer in 1887 [1]. Quantum Mechanics was a field that evolved out of new fine precision measurements of light and atoms during the first half of the twentieth century. The invention of the atomic clock has allowed for verification of the time-dilation effects predicted by Einstein's special relativity. In the future, large accelerators such as CERN will continue to collide particles at higher and higher speeds in the hopes of observing new and smaller particles. It is very difficult to think what physics would be like without the experimental observation and verification of quantum mechanics, special relativity, and particle physics.

Today, atomic clocks offer the finest dependable measurements of time. The best atomic clocks are based on the absorption spectra of cold alkali atoms. The international definition of the second is based off of a frequency transistion of Cesium-133, which is so accurate that these clocks are only off by 10^{-9} s/day. Yet to retain the accuracy of these clocks, the atomic transition must be measured while the atoms are in free fall. Thus these clocks have an accuracy of $1/\sqrt{T}$, where T is the time between atomic transition measurements, or in other words, the time it takes to throw up the atoms in the optical fountain clock and have them fall back to their original position.

Unfortunately, the very best atomic clocks are therfore very large.

There are several efforts underway to develop a clock of even finer precision, or one of equal precision but lower in cost and smaller in size. Clocks based on magnetically trapped atoms may allow for much longer measurement times T, since a precise magnetic field provides the standard for comparison and free fall is no longer required. In August 2004, a new chip-scaled atomic clock was demonstrated by NIST, which requires just 75 mW to run and is $1/100^{th}$ the size of traditional atomic clocks [27]. There is also much excitement over the possibility of using entangled atoms in these magnetic traps to decrease measurement noise. A magnetically trapped atomic clock using entangled atoms could achieve time-precision much finer than that of today's clocks based on independent particles, while still fitting on the lab table!

The Spin-Squeezing project in Vladan Vuletic's group at MIT proposes a scheme to reduce time-measurement uncertainty using entangled ^{87}Rb atoms prepared via optical cooling techniques. An atomic clock operates on the transition between two hyperfine energy levels. In this experiment, atoms are held in a magnetic microtrap long enough to allow their entanglement through spin-squeezing of the atomic clock transition. We are thereby working towards the potential for higher precision, more compact atomic clocks. This thesis serves as both a summary of the project in its current state, as well as a detailed reference for those specific components with which I have been more deeply involved since I began work on the project in September 2007.

This thesis consists of four main chapters and one appendix. Chapter 2 provides the theoretical background behind the spin-squeezing experiment and introduces several tools that will aid the reader to visualize our goals. Chapter 3 describes the experiment in detail, providing both an explanation of the major components of the system as well as a more general physical understanding for why it all works. Chapter 4 describes our preliminary observations of spin-squeezing. And in Chapter 5 we step back and evaluate the limitations and potentials for the experiment. In the appendix I will give specific details about a PID temperature controller I worked on this past year.

Chapter 2

Background Topics

2.1 Reduced Noise Limit

The precision of today's atomic clocks is at the standard quantum limit, where quantum projection noise is the largest noise component. Since projection noise is the result of random fluctuations in the proportion of N measured particles in a particular state after identical preparation, it follows a Poissonian distribution with signal-to-noise ratio: $SNR = N/\sqrt{N} = \sqrt{N}$. Therefore, the precision of today's atomic clocks scales as $1/\sqrt{N}$.

Spin-squeezing aims to make time measurements finer than that allowed by the standard quantum limit, approaching the Heisenberg limit where precision scales as $1/N$. Projection noise is reduced, since the wavefunctions of spin-squeezed atoms are correlated. J. M. Geremia et al. proposed a method capable of spin-squeezing using quantum feedback measurement in 2004 [2]. Our project aims to create entangled atoms using optical trapping and probing techniques.

2.2 Bloch Sphere Representation

To visualize the squeezing process, imagine the Bloch sphere for a two-state system, where the bottom point on the z-axis represents an eigenstate $|1\rangle$, and the antipodal point represents an eigenstate $|2\rangle$. All points in between are coherent superpositions

of eigenstates $|1\rangle$ and $|2\rangle$. Now extrapolate this Bloch sphere to represent the N-atom system, where the bottom point represents N atoms in the $|1\rangle$ state, and the opposite point has all N atoms in the $|2\rangle$ state. The state representation rotates in the xy-plane with time. In the standard quantum limit, there is some circle of uncertainty on the surface of the Bloch sphere. Figure 2-1 shows the case where $N/2$ atoms are in both the $|1\rangle$ and $|2\rangle$ states. Note that the Bloch sphere is frequently used in quantum mechanics to represent the angular momentum states [3]. Thus the Bloch sphere for N 2-level systems can also be viewed as the angular momentum distribution for a spin-$\frac{N}{2}$ system.

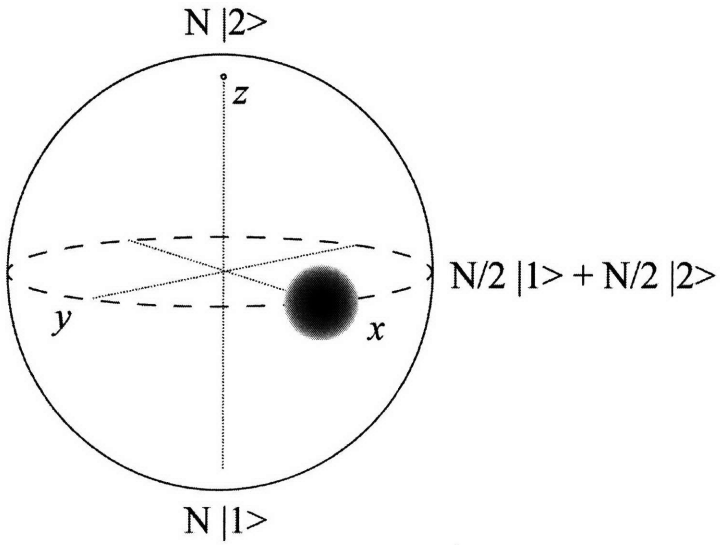

Figure 2-1: Bloch Sphere extrapolated to the N atom system. The south pole point represents the sphere where all N atoms are in the $|1\rangle$ state, and the north pole point is all N atoms in the $|2\rangle$ state. The atomic cloud shown here precesses in the xy-plane where approximately half the atoms are in state $|1\rangle$ and half are in state $|2\rangle$.

2.3 Spin Squeezing

2.3.1 Definition of Spin Squeezing

Spin or angular momentum systems can be represented by three cyclic noncommuting quantum operators $\mathbf{S} = (S_x, S_y, S_z)$. The Heisenberg uncertainty relationship states

that

$$\Delta\hat{S}_y\Delta\hat{S}_z \geq \frac{1}{2}|\langle\hat{S}_x\rangle|. \tag{2.1}$$

Thus the variances are related by

$$\langle S_i^2\rangle\langle S_j^2\rangle \geq \frac{1}{4}|\langle S_k\rangle|^2 \tag{2.2}$$

for spin states of eigenvalues S. Every measurement has uncertainty, with a minimum uncertainty limited by Equation (2.1).

Now assume we are at the minimum of the uncertainty relationship $\Delta\hat{S}_y\Delta\hat{S}_z = \frac{1}{2}|\langle\hat{S}_x\rangle|$. In our experiment, this is achieved with very cold atoms. When spins are uncorrelated, the uncertainty $S/2$ is evenly distributed in the directions normal to the mean spin vector, the (θ, ϕ) direction. This state with no quantum-mechanical correlations at the limit of the minimum uncertainty product is called the *coherent spin state* (CSS). Figure 2-2.a shows the distribution of the CSS for N spin-$\frac{1}{2}$ atoms on the Bloch Sphere. The CSS corresponds to an isotropic quasiprobability distribution (QPD) represented by a circle of radius $\sqrt{S/2}$.

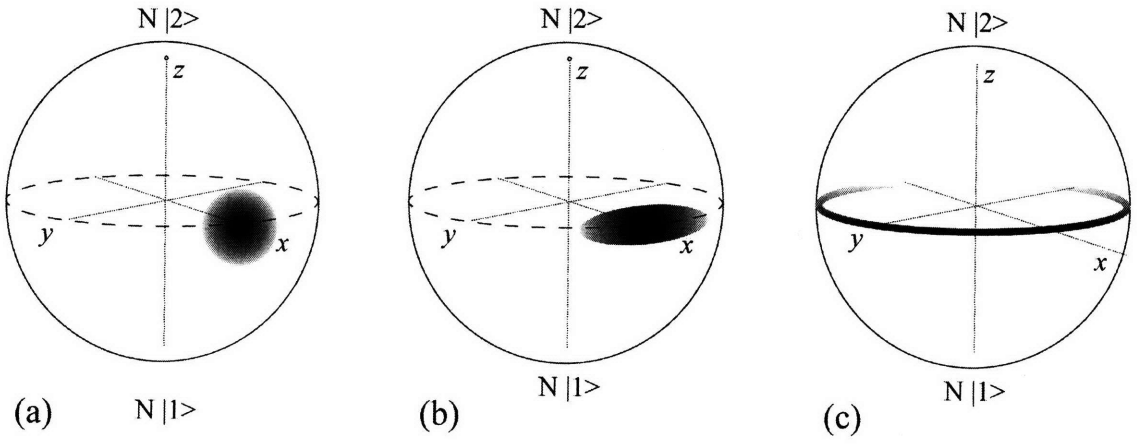

Figure 2-2: QPD representations on the Bloch Sphere for N spin-$\frac{1}{2}$ atoms. (a): All N spin-$\frac{1}{2}$ atoms are first in the unentangled coherent spin-state. (b): As atoms become more entangled, the uncertainty along the z-axis decreases, and the uncertainty circle streches into an ellipse. (c): When the ellipse stretches around the entire Bloch sphere, the Heisenberg limit is reached.

When there are quantum-mechanical correlations between spins, uncertainty fluctuations in one direction will be cancelled out, whereas fluctuations in an orthogonal direction will be enhanced. As a result, the variance of one spin component $\langle S_i^2 \rangle$ normal to the mean spin vector becomes lower than the standard quantum limit (SQL) $S/2$, and the state is defined to be a *spin squeezed state* (SSS). As individual spins become more entangled, the uncertainty along the z-axis decreases, and the CSS uncertainty circle stretches into an ellipse (Figure 2-2.b). The SSS has an elliptical quasiprobability distribution (QPD) like the cross section of a cone sliced on an angle. As squeezing continues, the QPD stretches further and further around the Bloch sphere. When the ellipse stretches entirely around the sphere so that no uncertainty remains in the z direction, the Heisenberg limit is reached.

2.3.2 One-Axis Twisting

Spin-squeezing is theoretically achieveable using nonlinear interaction methods as proposed by M. Kitagawa and M. Ueda [4]. I will first discuss the one-axis twisting method, as this is currently the only spin-squeezing method realizable in our experiment.

One-axis twisting consists of twisting the quasiprobability distribution (QPD) on the Bloch sphere about it's mean spin vector passing through its center. The distribution is thus transformed by the unitary operator $U(t) = exp[-itF(S_z)]$ created by some applied Hamiltonian $H = \hbar F(S_z)$ with arbitrary $F(S_z)$ [note $U(t)U^\dagger(t) = 1$]. The raising and lowering operators $S_\pm$ are

$$S_+(t) = U^\dagger S_+(0) U = S_+(0) exp[itf(S_z)] \tag{2.3}$$

$$S_-(t) = [S_+(t)]^\dagger \tag{2.4}$$

where $f(S_z)$ is defined as

$$f(S_z) = F(S_z + 1) - F(S_z). \tag{2.5}$$

A transformation proportional to S_z will result in a rotation about the x-axis and may be achieved by applying a Hamiltonian proportional to S_z^2.

$$F(S_z) = \chi S_z^2 \tag{2.6}$$

$$f(S_z) = 2\chi(S_z + \frac{1}{2}) \tag{2.7}$$

This particular f effectively "twists" the quantum fluctuations, shifting the uncertainty cloud in proportion to it's local S_z spin. A spin-squeezed state results. Fortunately, the Hamilitonian $H = \hbar\chi S_z^2$ is realizable in the laboratory. Our implementation of spin-squeezing via one-axis twisting will be explained in Section 4.3.

2.3.3 Two-Axis Countertwisting

The amount of spin-squeezing attainable via one-axis twisting, however, is limited by the geodesic swirliness of the QPD. Two-Axis countertwisting suggests a scheme to eliminate geodesic swirliness by rotating about one axis and counter-rotating around another axis [4]. In a manner similar to the spin-echo technique (Section 4.2), these two rotations cause the geodesic swirliness to cancel out. Hence, the QPD probability distribution is simultaneously rotated clockwise and counter-clockwise about two orthogonal axes normal to the mean spin vector. The necessary Hamiltonian is

$$H = \frac{\hbar\chi}{2i}(S_+^2 - S_-^2). \tag{2.8}$$

Reference [4] nicely compares the minimal uncertainty attainable by these two methods in the graph shown in Figure 2-3.

Two-axis countertwisting basically corresponds to the simultaneous excitation and deexcitation of two atoms. Unfortunately, no realistic physicial scheme has yet been realized for two-axis countertwisting. We therefore only implement one-axis twisting to obtain spin-squeezing.

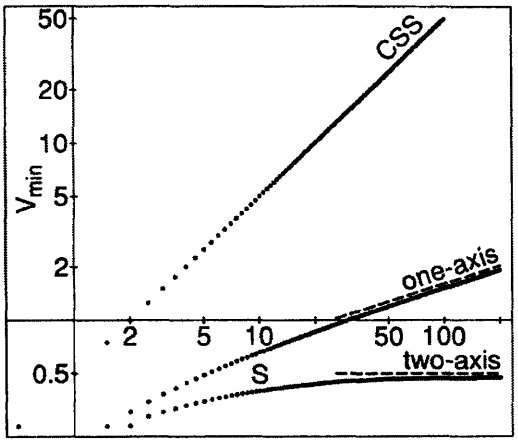

Figure 2-3: Minimal variance as a function of atomic number N. In the coherent spin state the variance scales as N. The minimal variance from one-axis twisting is far below that for a CSS, and for two-axis countertwisting it is even lower. The variance for two-axis countertwisting levels off at 0.5 for large N. Graph taken from Ref [4].

2.3.4 Quantum Non-Demolition Measurement

Now that it has been established that spin squeezing is theoretically possible, how would we actually detect spin-squeezing? We cannot simply observe the state of individual atoms, since such a disruption collapses the quantum wave function into a single eigenstate, leaving us once again at the standard quantum limit with unentangled atoms. Yet while we cannot find the exact properties of specific atoms, we can gather statistical information about a group of N indistinguishable atoms. A quantum non-demolition measurement (QND) is any technique that is able to indirectly measure a quantum system without collapsing its wavefunction. In this spin-squeezing experiment, we implement QND by measuring the relative proportion of atoms in each of two atomic states using an optical resonator of high finesse. The method will be described in greater detail in Section 4.4.

2.3.5 SSS Through Quantum Feedback Measurement

One problem in experimental quantum optics is that desirable states often correspond to highly unprobable measurement outcomes. Feedback measurements may be able to improve the probability for these unlikely outcomes via a partial measurement which

reduces the quantum uncertainty while still preserving the quantum wavefunction [2]. Since the quantum statistics of the measurement outcomes can be optimized by the appropriate intrameasurement feedback, these feedback-induced states are spin-squeezed.

Consider N atoms, each of whose total angular momentum as a result of nuclear spin, electron spin, and orbital angular momentum is represented by $\hbar f$. If all atoms are oriented along a common direction (say the x-axis), then the total angular momentum is $F = Nf$ and the net magnetization $\mathbf{F}$ is easily derived by:

$$\mathbf{F}^2 = \hbar^2 F(F+1) \tag{2.9}$$

$$|\mathbf{F}| = \hbar\sqrt{F(F+1)} \tag{2.10}$$

Equation (2.10) gives the eigenvalues of the net magnetization. The Heisenberg uncertainty relationship for the net magnitization $\mathbf{F}$ is

$$\Delta\hat{F}_y \Delta\hat{F}_z \geq \frac{1}{2}|\langle\hat{F}_x\rangle| \tag{2.11}$$

When all of the atoms are sufficiently cooled and aligned along the x-axis, $|\langle\hat{F}_x\rangle| = F$ and $\Delta\hat{F}_y = \Delta\hat{F}_z = \sqrt{F/2}$. This unentanged state is the coherent spin state prepared by optical pumping.

Reference [2] reported a spin-squeezed state resulting from the quantum feedback of the interaction between atomic magnetization and laser probe polarization. They observed a reduction in the F_z measurement with time over continual QND observation of one prepared state. Yet it is important to note that while feedback-induced spin-squeezing techniques reduce the measurement variance ΔF_z^2 of individual systems, they have no effect on the average measurements of multiple individually-prepared states.

As will be described in Seciton 4.6, we have achieved spin-squeezing by using quantum feedback measurement techniques in our experiment. Section 4.3 will describe the one-axis twisting technique we hope to implement soon. But unfortunately, we

do not currently have a scheme that allows us to realize two-axis countertwisting in our experiment.

Chapter 3

Experimental Setup

3.1 Overview

Our spin-squeezing experiment consists of a ^{87}Rb source, a magneto-optical trap (MOT), an optical cavity around a microtrap, and magnetic coils to transport atoms from the source to the cavity (Figure 3-2) within a vacuum chamber. Multiple lasers are needed to cool and confine the atoms, to probe them, and to control for noise.

First, about 10^5 ^{87}Rb atoms are optically pumped into the same trappable spin-state $|1\rangle$ for about five seconds. Next, a magnetic field produced by the coils raises the atoms from the MOT to the optical cavity, where they are optically and magnetically confined to a small volume for a relatively long measurement time (ms to s). The MOT beams are turned off. A $\pi/2$ microwave pulse applied to the atoms shifts them into a superposition state of $|1\rangle$ and $|2\rangle$. In the Bloch Sphere picture, the $\pi/2$ pulse is equivalent to moving the uncertainty circle from the bottom of the Bloch sphere to some position on the surface of the Bloch sphere where $z = 0$ (Figure 3-1).

The entangled state is allowed to precess for some time t before another $\pi/2$ microwave pulse is applied and the cavity is probed to measure the proportion of atoms in each of the two states. The application of the microwaves combined with precession times takes about 5 ms. An additional 300 ms is needed to ramp down the current in the magnetic coils to disperse our atoms in preparation for the next round of measurements. Thus each round, which consists of loading and trapping

atoms, atom manipulation and measurement, and dumping the trapped atoms, takes between 5 and 10 seconds.

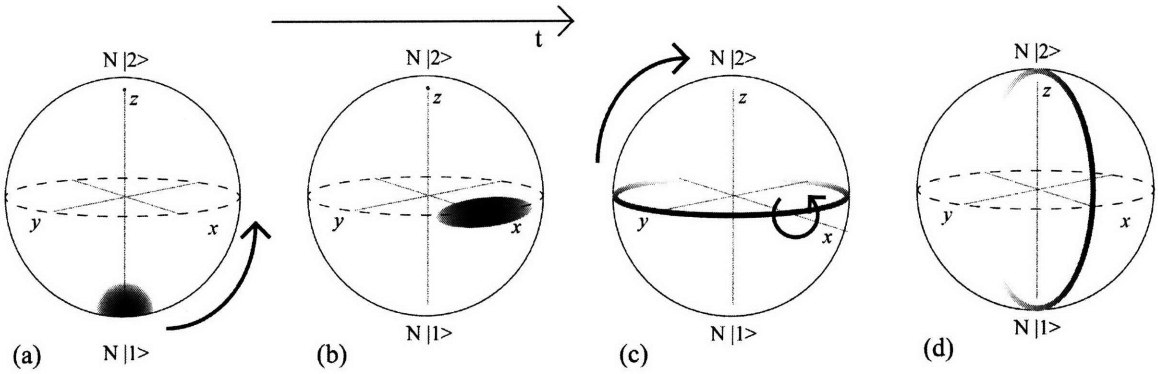

Figure 3-1: Effects of microwave pulses on atomic state distribution. (a): All of our atoms are first optically pumped into the $|1\rangle$ state. (b): A $\pi/2$ pulse rotates the atoms into the entangled $|1\rangle + |2\rangle$ state. (c): The atoms are spin squeezed over a time t and then rotated about their mean spin vector by a $\pi/2$ pulse. Image (d) shows a spin-sqeezed state that may be used for precise phase measurement.

3.2 The Lasers

Figure 3-2 diagrams the laser paths through the MOT. Three 852 nm MOT laser beams cross within the MOT just above the surface of the microchip, creating a dipole trap. These three beams are positioned to cover three orthogonal directions. A trap laser beam creates a dipole trap within the optical cavity around the microchip. The probe and cavity laser beams are also aligned to pass through the optical cavity. The cavity beam together with a lock laser beam counteract vibrations and thermal fluctuations by adjusting the distance between the cavity mirrors to maintain a constant cavity resonance frequency (Pound-Drever lock scheme). The probe beam is detuned from the cavity resonance and is used to measure the atoms in the cavity. All of the beam frequencies are based off of one reference laser. Additionally, each individual diode laser is frequency-locked by a lock-box and temperature stabilized using a PID current controller. More information on the PID controller is provided in Appendix A.

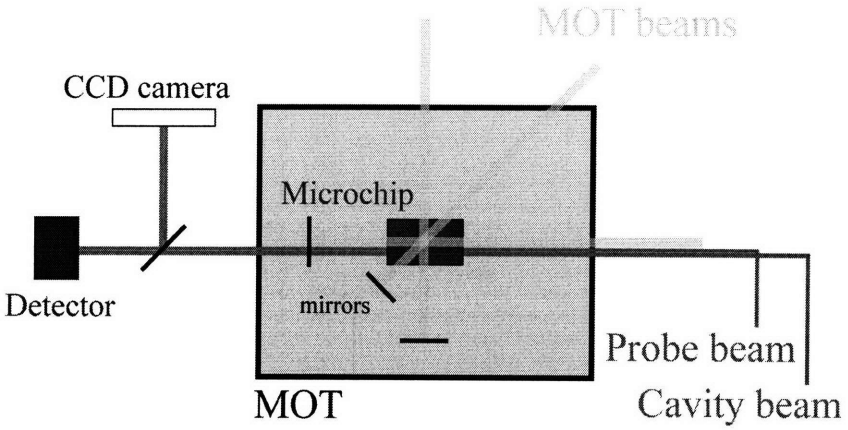

Figure 3-2: Diagram of the laser paths through the MOT.

3.2.1 Acousto-Optic Modulator (AOM)

An acousto-optic modulator (AOM) uses sound waves to alter the refractive index of a material and thus diffract and shift the frequency of incoming light. An AOM consists of a highly transparent crystal or glass sandwiched between a piezo-electric transducer and an acoustic-absorbing slab (Figure 3-3). An oscillating electric signal applied to the piezo-electric transducer causes sound waves to vibrate through the transparent material, periodically altering the refractive index and effectively creating a periodic diffraction grating. Photons from an incoming laser beam interact with the lattice through Brillouin scattering, a process by which a phonon is either created or destroyed. The scattering between photons and the periodically varying density of phonons in the crystal generates at scattering pattern very similar to that for Bragg diffraction:

$$sin\theta = \frac{m\lambda}{2\Lambda}, \tag{3.1}$$

where Λ is the wavelength of sound, λ is the wavelength of the incoming light, and m is the order of refraction. Because of this similarity, the AOM is also referred to as the Bragg cell.

The intensity, phase, direction, and frequency of the outcoming laser beam may be adjusted by varying the applied electric signal. The amount of light refracted

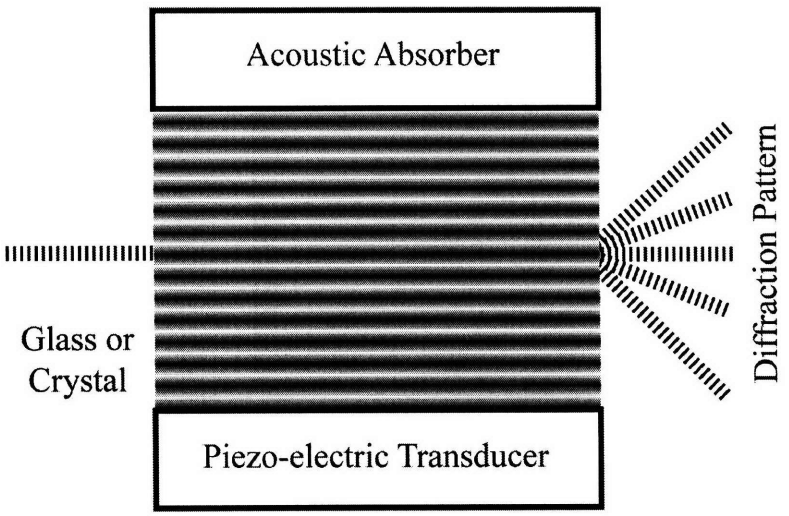

Figure 3-3: An Acousto-Optic Modulator (AOM) consists of a highly transparent crystal or glass sandwiched between a piezo-electric transducer and an acoustic-absorbing slab. An oscillating electric signal applied to the piezo-electric transducer causes sound waves to vibrate through the transparent material, periodically altering the refractive index and effectively creating a periodic diffration grating.

depends on the intensity of the sound waves. When light is scattered off of moving planes, it experiences a doppler shift $\nu \rightarrow \nu + m\nu_s$, where ν_s is the frequency of the sound waves. Thus an AOM can slightly alter the frequency of incoming light. Note that a standing wave will not create a doppler shift, in the event that a frequency shift is not desired. In our setup, we use AOMs to quickly adjust the intensity of the incident laser beams. With our AOMs, we are able to change the intensity as quickly as every ten nano-seconds.

AOMs have many applications to laser science. They are useful for Q-switching of solid-state lasers, active mode-locking, and for the generation of ultrashort laser pulses with high peak power. They are used as signal modulators in telecommunications and in laser printers. Additionally, they can allow for fine frequency control of spectroscopy measurements [5].

3.3 Magneto-Optical Trap (MOT)

A Magneto-Optical Trap (MOT) is a vacuum chamber that can trap and cool atoms to near absolute zero using a combination of magnetic fields and circularly polarized light. On the outside of the chamber, magnetic coils are arranged in an anti-Helmholtz configuration, which creates a zero magnetic field minimum at the center of the trap [6]. Three retroreflected orthogonal laser beams cross over the field minimum within the cavity [7].

3.3.1 Doppler Effect

When an atom is in motion, the frequency of an atomic transtion is shifted according to the Doppler effect. The photon resulting from a transition between the E_2 (excited) and E_1 (ground state) energy levels has an energy $\hbar\omega = E_2 - E_1$. Conservation of energy and momentum for an atom moving at speed v results in

$$\hbar\omega' = \frac{\hbar\omega}{1 - (v/c)\cos\theta}, \tag{3.2}$$

where θ is the angle between the direction of the velocity and that of the photon. Equation 3.2 corresponds to a frequency shift of

$$\Delta\omega = \omega\frac{v}{c}\cos\theta. \tag{3.3}$$

Doppler broadening can be quite significant at high temperatures. Yet the doppler broadening can be almost completely eliminated if the motion of the atoms is restricted to a region that is small compared to the wavelength $\lambda = \frac{2\pi c}{\omega}$ of the photons (Dicke regime [8]). Alternatively, if the atoms are restricted to a region of constant phase, such as a microwave cavity, then the Doppler broadening is also greatly reduced. [9]

3.3.2 Trapping Mechanism

A field minimum combined with photon interactions is essential to trapping and cooling neutral atoms in a MOT. Two effects are at play in the interaction: Doppler cooling, due to frequency variations of scattered light because of the Doppler effect (Section 3.3.1), and energy resonance due to the Zeeman splitting of energy levels.

In Doppler cooling, when an photon of wavevector $\mathbf{k_i}$ interacts with an atom of mass m, scattering a photon of wavevector $\mathbf{k_s}$, the atom's energy changes from $W = \mathbf{p}^2/2m$ to

$$W' = \frac{(\mathbf{p}')^2}{2m} \tag{3.4}$$

$$= \frac{(\mathbf{p} + \hbar\mathbf{k_i} - \hbar\mathbf{k_s})^2}{2m} \tag{3.5}$$

$$= W + \hbar(\mathbf{k_i} - \mathbf{k_s}) \cdot \mathbf{v} + \frac{\hbar^2(\mathbf{k_i} - \mathbf{k_s})^2}{2m}. \tag{3.6}$$

Therefore the change in angular frequency of the incident photon is

$$\Delta = \frac{W - W'}{\hbar} = -(\mathbf{k_i} - \mathbf{k_s}) \cdot \mathbf{v} - \frac{\hbar(\mathbf{k_i} - \mathbf{k_s})^2}{2m}. \tag{3.7}$$

In the above expression there are two energy-altering terms. $-(\mathbf{k_i} - \mathbf{k_s}) \cdot \mathbf{v}$ is the two-photon Doppler effect, and $-\frac{\hbar(\mathbf{k_i}-\mathbf{k_s})^2}{2m}$ describes the recoil heating which is independent of atomic velocity. The atomic gas is cooled if $\Delta > 0$, and the average Doppler effect term is negative. Because there is scattering in all directions, $\mathbf{k_s} \cdot \mathbf{v} \geq 0$; therefore, $\langle \mathbf{k_i} \cdot \mathbf{v} \rangle$ must be negative for cooling to occur. This can be implemented using a laser beam tuned below the frequency of the atomic transition of interest. Therefore, a detuned laser beam decreases the momentum of atoms traveling towards it due to the relativistic Doppler shift. [10]

Additionally, the further an atom is from the minimum of the magnetic trap, the more its energy is shifted by the Zeeman effect, bringing its energy closer into resonance with the detuned laser passing through the chamber. These far-out atoms experience more scattering from the laser beam and thus have an increased probability

of Doppler cooling. Hence, three laser beams aligned orthogonally to cover the three spatial directions effectively slow down the atoms and push them to the magnetic minimum of the trap. Thus in our MOT we implement Doppler cooling, and the atoms are simultaneously magnetically trapped and Doppler cooled in the MOT.

A MOT is crucial as a first-stage cooling mechanism for neutral atoms, and is thus important to many cooling experiments involving the formation of Bose-Einstein condensates or other ultra-cold atoms. The MOT also has several other important applications and has been responsible for some of the finest measurements of the CP violation and detections of relative quantities of various isotopes.

3.4 The Magnetic Microtrap

A magnetic microtrap can trap neutral atoms due to their intrinsic atomic magnetic moment. The presence of a magnetic field causes a Zeeman shift in the atom's energy that is proportional to the magnetic moment μ in the direction of the magnetic field **B**.

$$\Delta E = -\mu * \mathbf{B} \tag{3.8}$$

Thus, atoms whose magnetic moments are aligned with the magnetic field have the lowest energy in high fields, and atoms whose magnetic moments are oppositely aligned have the lowest energy in low fields. These two types of atoms are called high field-seeking and low field-seeking atoms, respectively. The tendency for atoms to seek high-field or low field areas allows for the trapping of atoms by a local magnetic field minimum or maximum. A local magnetic field maximum cannot be produced in free space; however, a local non-zero magnetic field minimum can. Therefore, the purpose of the magnetic microtrap is to create a magnetic field minimum to trap atoms. [11]

An 852 nm laser creates a local dipole trap near the magnetic field minimum. The magnetic field gradient may then transformed adiabatically into an Ioffe-Pritchard microtrap near the surface of the chip, disrupting the anti-Helmholtz field configuration to create a local non-zero magnetic field minimum where the ^{87}Rb atoms are trapped.

The minimum in the magnetic field falls along the center bar in Figure 3-4, and its position may be adjusted by varying the current through the chip.

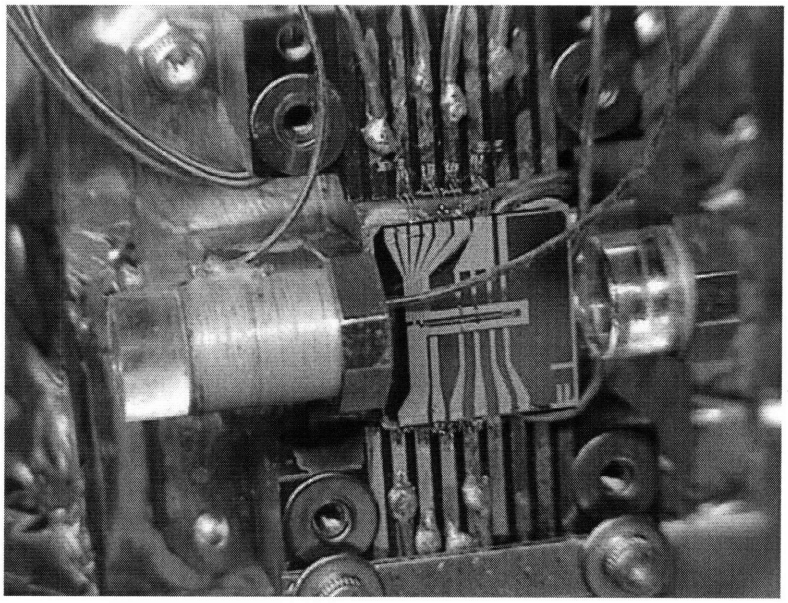

Figure 3-4: Our magnetic trap creates a local dipole trap near the magnetic field minimum. The magnetic field gradient is then transformed adiabatically into an Ioffe-Pritchard microtrap near the surface of the chip, disrupting the anti-Helmholtz field configuration to create a local non-zero magnetic field minimum where the ^{87}Rb atoms are trapped. The minimum in the magnetic field falls along the center bar, and its position may be adjusted by varying the current through the chip. Image taken from Reference [12].

The chip is created using a combination of photolithography and wet etching techniques. Several thin layers of metal bind 100 nm thick gold wires to a dielectric silicon substrate covered with an insulating Si_3N_4 diffusion barrier [13]. In general, microtraps consist of a very thin conductor of low magnetic field noise on a dielectric surface.

Microfabricated magnetic traps are an important component of quantum information processing, since they may be fabricated to generate tight and complicated magnetic fields that are able to control atoms very precisely. Steep potential traps magnetically compress atomic gases, allowing for high elastic two-body collision rates that rapidly thermalize atoms. The result is reduced cooling time for BEC formation and the possibility to cool artificial or radioactive particles via evaporative cooling

[14]. The magnetic microtrap was first proposed as a method to cool atoms by David Pritchard of MIT in 1983 [15]. Note that microtraps only work as a last stage in cooling, since their shallow field minima are usually only able to trap atoms less than a milli Kelvin. Many other possible applications of microfabricated magnetic traps are also currently being explored by scientists. They have the potential for more accurate atom interferometry, new types of atomic clocks, as Bragg reflectors, or as Josephson junctions [13].

3.5 Cooling the Atoms

It is extremely important that we work with very cold atoms, since warmer atoms experience thermal motion that limits our ability to precisely control them. Thermal motion leads to a broadening of the resonance lines and thereby decreased precision.

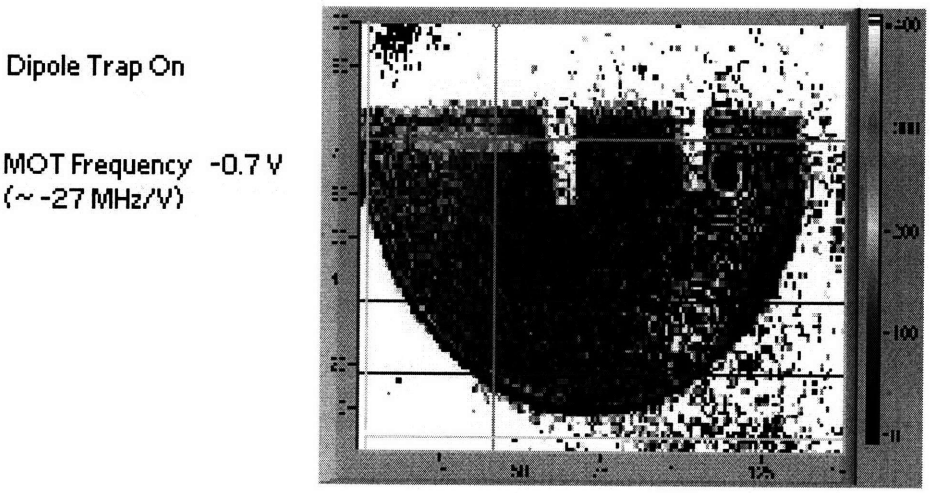

Figure 3-5: Profile of the trapped cylindrical atomic cloud taken with a CCD camera. When fully cooled the cloud contains about 10^5 atoms and is approximately 1 mm by 10 μm in size.

Figure 3-5 is the elliptical profile of the trapped atomic cloud. When fully cooled, the cloud contains about 10^5 atoms and is approximately 1 mm by 10 μm in size. Images such as this one were taken with a CCD camera while adjusting the MOT laser beams to optimize the size and position of the atomic cloud.

3.5.1 Degenerate Raman Sideband Cooling

We are currently preparing our atoms via optical molasses. However, we will be able to cool our atoms even further if combine 3D degenerate Raman sideband cooling with optical pumping to prepare trappable states.

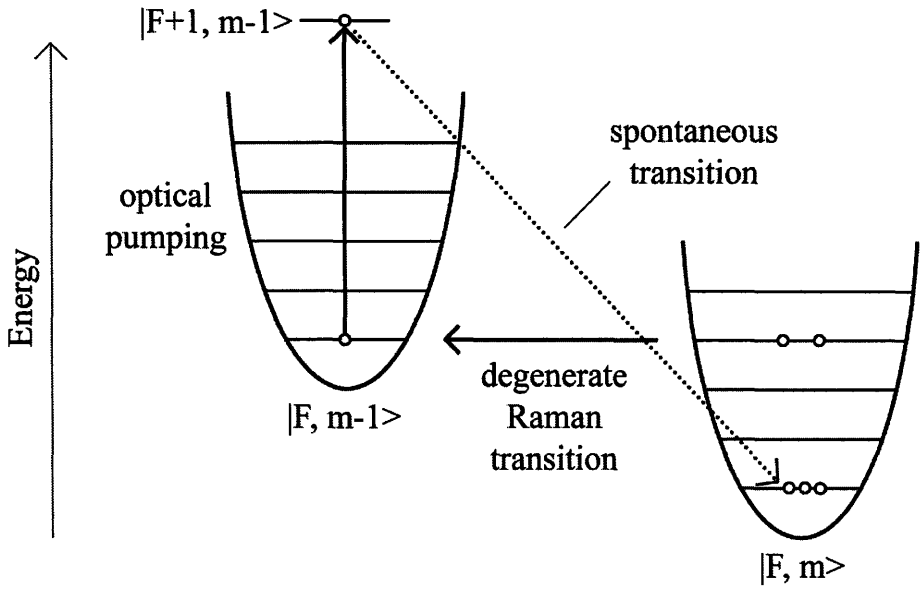

Figure 3-6: Preparation of an atomic clock transition state: Excited vibrational states freely transition between degenerate energy levels via 3D degenerate Raman sideband transitions. Atoms are then optically pumped into a higher state where they spontaneously decay. The difference in the vibrational ground states is due to Zeeman splitting.

Excited vibrational states freely transition between degenerate energy levels via a process called 3D degenerate Raman sideband cooling. After transition, these atoms are optically pumped by a laser into higher energy states where they may spontaneously decay to the vibrational ground state of $|1,-1\rangle$, a state that is "dark" to both Raman transitions and optical pumping. These spontaneous transitions occur at a specific frequency and may provide the basis for an atomic clock. The cooling scheme is diagrammed in Figure 3-6 [16].

Raman sideband cooling may only be used in the Lamb-Dicke regime, where the wavelength of the ground state wavefunction is less than the wavelength of the atomic transition. In this case, photons are scattered off the atom without changing

the atom's momentum, and the spacing between vibrational energy levels will greatly exceed the recoil energy [16].

This two-step method is far superior to evaporative cooling, which tends to be slow and remove most of the atoms. Thus degenerate Raman sideband cooling combined with optical pumping in a MOT allows for quick cooling of many atoms.

Chapter 4

Observing Spin-Squeezing

4.1 Lorentzian Lineshape of Cavity Resonance

The lineshape of the cavity resonance is a Lorentzian due to the finite cavity lifetime. Figure 4-1 shows a sample cavity resonance from a frequency spectroscopy measurement. The Lorentzian on the right is the resonance of the empty cavity. The presence of atoms within the cavity shifts the cavity resonance to the left, as shown by the Lorentzian on the left.

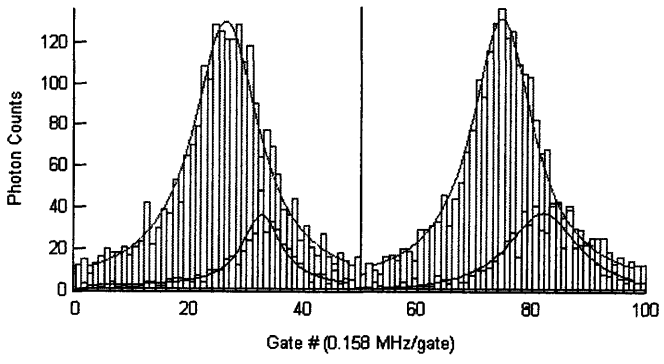

Figure 4-1: Sample cavity lorentzian: The lorentzian on the right is the resonance of the empty cavity. The index of refraction within the cavity is atomic state dependent. The lorentzian on the left is the shifted cavity resonance resulting from the presence of atoms in various atomic states.

4.2 Spin-Echo Measurement

Due to their various positions along the probing laser, not all of the atoms are exposed to the same intensity of light. This leads to a dephasing of the atomic states as they precess in the xy-plane. For long precession times, this dephasing is very significant and can greatly increase the area of the quasi-probability distribution (QPD). We thus implement a Spin-Echo technique to cancel out these dephasing effects. First the QPD is allowed to precess in one direction for a time $t/2$. A π pulse is applied to the atoms, causing them to then precess in the opposite direction. After precession in this direction for another time $t/2$, the dephasing effects have been cancelled out. We then take our measurement.

4.3 One-Axis Spin-Squeezing Technique

We are able to implement spin-squeezing via a one-axis twisting method, since interactions between the probe beam and the atoms give rise to differential light shifts due to the AC Stark effect. It is possible to apply a Hamilitonian of the form $H \propto S_z^2$ to our atoms via a Stark shift that is directly proportional to the difference in atom number between the two states of interest.

Since the lineshape of the cavity resonance is a Lorentzian, its slope around half-maximum intensity is approximately linear. The probe beam is slightly detuned from the cavity resonance frequency, so that it intercepts the cavity resonance near its half-maximum. Since the index of refraction within the cavity is dependent on atomic state, the resonance frequency of the cavity shifts based on the number of atoms in the two states. An atom in the $F = 2$ state shifts the intercept point to the right, whereas an atom in the $F = 1$ state shifts it to the left. The intensity I of the interaction is therefore proportional to the difference between the number of atoms in the two states. Thus, $I \propto N_2 - N_1$.

Let N_2 be the number of atoms in $F = 2$ energy level and N_1 be the number of atoms in $F = 1$ energy level. The energies E_2 and E_1 of the $F = 2$ and $F = 1$ energy

levels are shifted by the AC Stark effect to become

$$E_2 = E_2^0 + c(N_2 - N_1) \tag{4.1}$$

$$E_1 = E_1^0 - c(N_2 - N_1). \tag{4.2}$$

The total energy of N atoms is therefore

$$E = N_1 E_1 + N_2 E_2 \tag{4.3}$$

$$= N_1[E_1^0 - c(N_2 - N_1)] + N_2[E_2^0 + c(N_2 - N_1)] \tag{4.4}$$

$$= N_1 E_1^0 + N_2 E_2^0 + c(N_2 - N_1)^2 \tag{4.5}$$

$$= E^0 + c(N_2 - N_1)^2. \tag{4.6}$$

From the Bloch sphere representation, we know that $N_2 - N_1 = S_z$. Therefore the energy shift is

$$\Delta E = E - E^0 = cS_z^2, \tag{4.7}$$

and we have realized the perturbation Hamiltonian $H \propto S_z^2$ necessary for one-axis spin-squeezing. The interaction between the atoms and a slightly detuned probe laser beam thereby causes the spin-squeezing of our atoms.

4.4 Implementation of QND

The state of the atoms must be measured without directly observing the state of individual atoms; otherwise the quantum wave function collapses into a single eigenstate, and we are once again at the standard quantum limit. Since the atoms in the optical resonator are indistinguishable, a measurement of the proportion of atoms in each of the two atomic states preserves the symmetry of the quantum wave function, while creating a squeezed state. The index of refraction of the atoms is state-dependent, so this proportion may be measured by observing the phase shift of a probe beam that is near-resonant to an optical resonator. The optical cavity has a high finesse of 5600 at the 780 nm region where we are currently probing and an optimum cavity finesse

of 40000 at 852 nm.

4.5 Rabi Cycle and Ramsey Oscillations

The Rabi cycle is the cyclic behavior of a 2-level system between excitation and de-excitation. The probability to find an atom in the excited state is $|p_2(t)|^2 = cos(\Omega t)^2$, where Ω is the frequency of oscillation, called the Rabi frequency (analogous to Larmor precession frequency) and t is the precession time. [17]

The coherence lifetime of our atoms is a measure of the decoherence of the atomic cloud on the Bloch sphere. It is important to measure the coherence lifetime of our atoms, so that we know the time frame in which we can perform experiments with entangled atoms. The lifetime is mostly limited by interactions between the atoms and the trap laser.

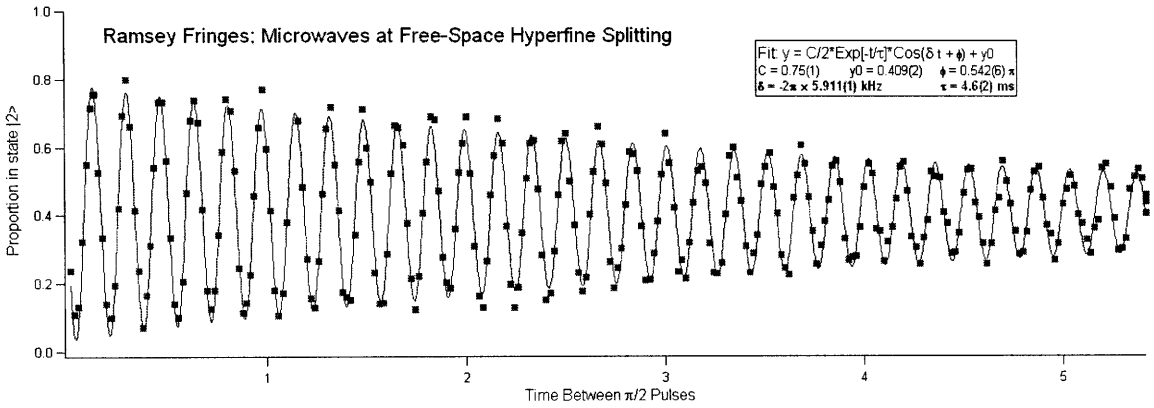

Figure 4-2: Ramsey spectroscopy of our atoms. We found the coherence lifetime to be 4.6(2) ms.

The coherence lifetime is found by measuring the damping coefficient in Ramsey spectroscopy. The atoms are prepared in a ground state $|1\rangle$. A $\pi/2$-pulse rotates the atoms into an equal superposition of $|1\rangle$ and $|2\rangle$ states. The atoms are allowed to precess for a time t. Then another $\pi/2$-pulse is applied, and the atomic cloud is probed. The proportion of atoms in state $|2\rangle$ is then found by analyzing the shift in the cavity resonance [18]. Figure 4-2 shows our measurements of Ramsey oscillations

for the $(F = 2, m_F = 0) = |2\rangle$ to $(F = 1, m_F = 0) = |1\rangle$ transition. Each data point is the result of one complete measurement sequence: loading the atoms, applying microwave pulses, probing, and dumping the atoms. The distance between peaks corresponds to the detuning. The exponential decay of the oscillations is due to the decoherence of the atoms, so the damping coefficient is thereby a measurement of the coherence lifetime. Our coherence lifetime for the data presented in Figure 4-2 is 4.6(2) ms. We have improved the coherence lifetime to about 10 ms.

Figure 4-3 shows changes in the cavity resonance frequency during one measurement cycle. First the atoms are prepared in the $|1\rangle$ state. A microwave pulse is applied to the atoms, and the atoms oscillate between states $|1\rangle$ and $|2\rangle$ at their Rabi frequency. Then another microwave pulse is applied to return the atoms to the $|1\rangle$ state. The atoms are repumped with a π-pulse to the $|2\rangle$ state, and then are blown away.

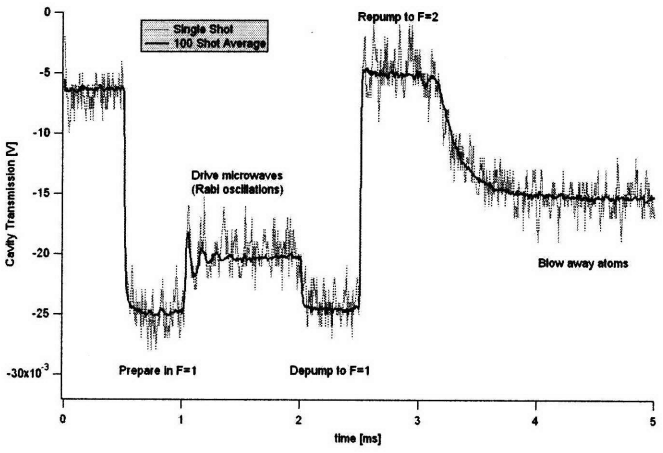

Figure 4-3: Changes in the cavity resonance frequency during one measurement cycle.

4.6 Spin-Squeezing: First Measurements

Figure 4-4 shows spin-squeezing of the $(F = 2, m_F = 0) = |2\rangle$ to $(F = 1, m_F = 0) = |1\rangle$ transition using partial measurement. Spin-squeezing was achieved using a sequence of two measurements. The first observes an approximate *coherent spin-*

state (CSS) in the $|1\rangle + |2\rangle$ region of the Bloch sphere. The second observes the effects of the first measurement on the CSS atoms. The red crosses in Figure 4-4 are the first measurements of the CSS, and the blue squares are the second measurements. The smaller variance for the second measurements shows that the first measurements effectively spin-squeezed the atoms! The additional green line is based on the photon shot noise limit and demonstrates the level of squeezing we could theoretically achieve

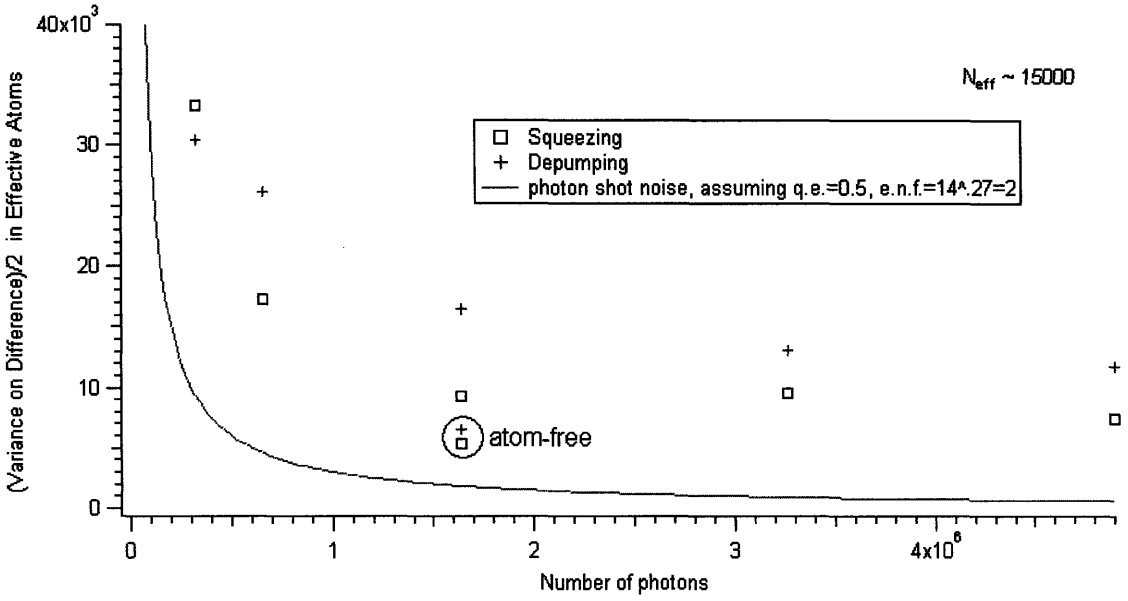

Figure 4-4: Spin-squeezing of the ($F = 2$, $m_F = 0$) to ($F = 1$, $m_F = 0$) transition: The red crosses are the first spin-echo measurements of the CSS, and the blue squares are the second measurements. The smaller variance for the second measurements shows that the first measurements effectively spin-squeezed the atoms! The additional green line is based on the photon shot noise limit and demonstrates the level of squeezing we could theoretically achieve.

4.7 Spin-Squeezing: Atomic Clock

Our first measurements of spin-squeezing are for the atomic transition ($F = 2$, $m_F = 0$) to ($F = 1$, $m_F = 0$). The $m_F = 0$ states are magnetic field insensitive to first-order approximation, so we are able to measure transition frequency extremely precisely. However, it is very difficult to make a frequency standard out of the $m_F = 0$ states,

since there are several factors that shift energy levels in a way that cannot be easily controlled in the lab.

It is much better to use magnetically trappable states, since their transition frequency is field-dependent. The Zeeman shifts for the for the $F = 2$ and $F = 1$ hyperfine states of the $5S_{1/2}$ orbital varies with magnetic field according to the Breit Rabi formulas. There is a special spot around 3.23 G where the ($F = 2$, $m_F = 1$) and ($F = 1$, $m_F = -1$) hyperfine levels experience the same Zeeman shift to first-order approximation [19]. Thus, there is a a region where the Zeeman shift is relatively stable against small changes in the magnetic field, allowing for dependable transition frequency measurements. The experimental demonstration by Harber et al. of this stability region is shown in Figure 4-5.

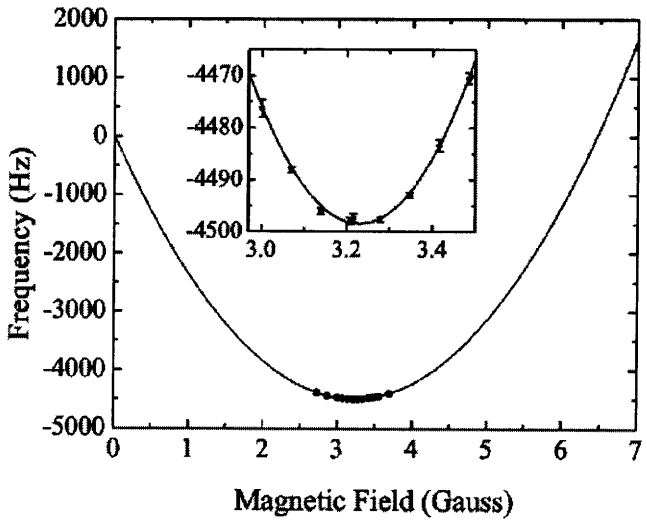

Figure 4-5: The Zeeman splitting is relatively constant around 3.23 Gauss magnetic field. Graph taken from Reference [19].

As mentioned in Section 3.4, a magnetic field minimum can trap atoms whose magnetic moments are oppositely aligned to the magnetic field. Thus the ($F = 2$, $m_F = 2$), ($F = 2$, $m_F = 1$), and ($F = 1$, $m_F = -1$) states are all trappable in a magnetic field minimum. We hope to ultimately show spin-squeezing in the ($F = 2$, $m_F = 1$) to ($F = 1$, $m_F = -1$) transition, a magnetically trappable state which could be the basis for an actual atomic clock. Yet while the trapping of $m_F = 0$ states

requires a dipole trap created by a light field, the $|1,-1\rangle$ and $|2,1\rangle$ states may also be trapped magnetically.

Chapter 5

Discussion and Outlook

5.1 Limits on Precision

While we are able to achieve a spin-squeezed state below the shot-noise limit, we are still far from the Heisenberg limit. There are several technical obstacles that limit our measurement precision.

Our most serious technical obstacle is cavity frequency noise. Even the smallest vibrations or thermal variations will slightly alter the resonance frequency of the optical cavity. Fortunately, we are able to integrate a large-bandwidth Pound-Drever lock scheme to offset most of the cavity frequency noise. This scheme locks the cavity to a far off-resonant laser while continuously adjusting the distance between the cavity mirrors. Some cavity frequency noise still remains, but it is greatly reduced by the Pound-Drever lock. [20]

5.2 Future of the Experiment

We are currently measuring spin-squeezing for the atomic transition ($F = 2$, $m_F = 0$) $\rightarrow$ ($F = 1$, $m_F = 0$), since the $m_F = 0$ states are the easiest to trap and cool. The $m_F = 0$ states, however, cannot be used as a frequency standard for an atomic clock, since their transition frequencies are dependent on several variables which are difficult to control. Therefore, the next step is to measure spin-squeezing on the transition

between the magnetically trappable states ($F = 2$, $m_F = 1$) and ($F = 1$, $m_F = -1$). These states experience a relatively constant transition frequency around 3.23 Gauss [19]. The preparation of magnetically trappable states will also require degenerate Raman sideband cooling and optical pumping [16].

As mentioned in Section 4.2, interactions between the atoms and the probe beam causes a dephasing of the QPD due to different atoms seeing different beam intensities. We thus plan to take only spin-echo measurements in the near future.

Also, right now we are only cooling our atoms using optical pumping. Degenerate Raman sideband cooling will allow us to cool our atoms to lower temperatures. We are able to implement this cooling mechanism with our experimental setup, but as a first step we have prepared our atoms via optical pumping alone.

Spin-squeezing of our atoms is achieved by partially measuring the atomic states. Instead of measuring the states of individuals atoms, we measure the proportion of atoms in each of two states, thereby making a quantum non-demolition measurement. Ultimately, we aim to create spin-squeezing via the one-axis twisting scheme described in Section 4.3. This method would sqeeze the atoms through the AC Stark shift induced by an incident laser. If there was a way to experimentally implement two-axis counter-twisting, we could further reduce our measurement uncertainty, approaching the Heisenberg limit.

Concluding Remarks

A good understanding of spin-squeezing will allow physicists to describe many correlated physical systems. Quantum dots and Cooper pairs in superconductors act like correlated systems; as do macroscopic two-state quantum systems such as interferometers and Josephson junctions. Spin-squeezing also offers the potential for improved sensitivity of spin-resonance measurements, including magnetometry and atomic clocks.

The described spin-squeezing experiment opens new doors for increased clock precision using the unintuitive laws of entanglement in quantum physics. Many-

particle entanglement is absolutely fundamental to quantum information science [21]. If sucessful, the study of spin-squeezed atomic transitions could ultimately lead to the implementation of high-precision portable clocks.

Appendix A

PID Temperature Controller

A proportional-integral-derivative (PID) controller uses proportional, integral, and derivative gains to continuously correct for the error between a measured variable and a setpoint. Each of our lasers requires a PID controller to stabilize its temperature. Figure A-1 shows the circuit diagram for the new temperature controller design I set up this year.

PID controllers correct for error, $\varepsilon(t) = \textit{setpoint - measured variable}$, based on the sum of proportional, integral, and derivative correction terms:

$$\Delta E_C = P_C + I_C + D_C. \tag{A.1}$$

The proportional correction term is

$$P_C = k_p \varepsilon(t). \tag{A.2}$$

A higher proportionality gain k_p results in a quicker response; however, if the proportional gain is too high, the system will experience instability and possibly oscillatory behavior.

The integral correction term is

$$I_C = k_i \int_0^t \varepsilon(t) dt. \tag{A.3}$$

Integral gain is important for correcting any small steady-state error. Again, a higher integral gain k_i also results in a quicker response. Yet because the integral correction cumulates error, an integral gain that is too large will cause the system to greatly overshoot the desired setpoint.

And the derivative correction term is

$$D_C = k_d \frac{d\varepsilon}{dt}. \tag{A.4}$$

The derivative term acts to slow the correction rate, and it is most significant when the error $\varepsilon(t)$ is small. Thus, this term has the greatest effect near the setpoint. [22]

Table A.1 summarizes the effects of increasing each of the gain parameters.

Table A.1: Result of increasing gain parameters [22]

Gain	Reaction Time	Amount of Overshoot	Settling Time	Steady-State Error
k_p	decrease	increase	small change	small decrease
k_i	decrease	increase	increase	eliminate
k_d	small decrease	decrease	decrease	none

The object is to adjust the current applied to the lasers so that the temperature stabilizes quickly and has only very minimal deviations from the desired setpoint. Variable resistors on the circuit board are manually adjusted to maximize the temperature stability of each laser. First, the integral and derivative gains are set to zero, and the proportional gain is adjusted until the system oscillates. Then all three components may be fined-tuned. The temperature setpoint is pre-determined by two external controls. Course adjustment of the setpoint is provided by a resistor switch box containing resistors from 10-100 $k\Omega$; fine adjustment is then achieved with a precision potentiometer.

A proportional control alone will not be able to reach the setpoint, since the error is non-zero in the steady state. The addition of an integral gain increases reaction time while eliminating steady state error. Yet only a derivative control will allow the system to truly stabilize, since it may slow the oscillations near the setpoint. The derivative control, however, is extremely sensitive to measurement noise, so we only

use propotional and integral gains (PI controller) to stabilize the current applied to our lasers.

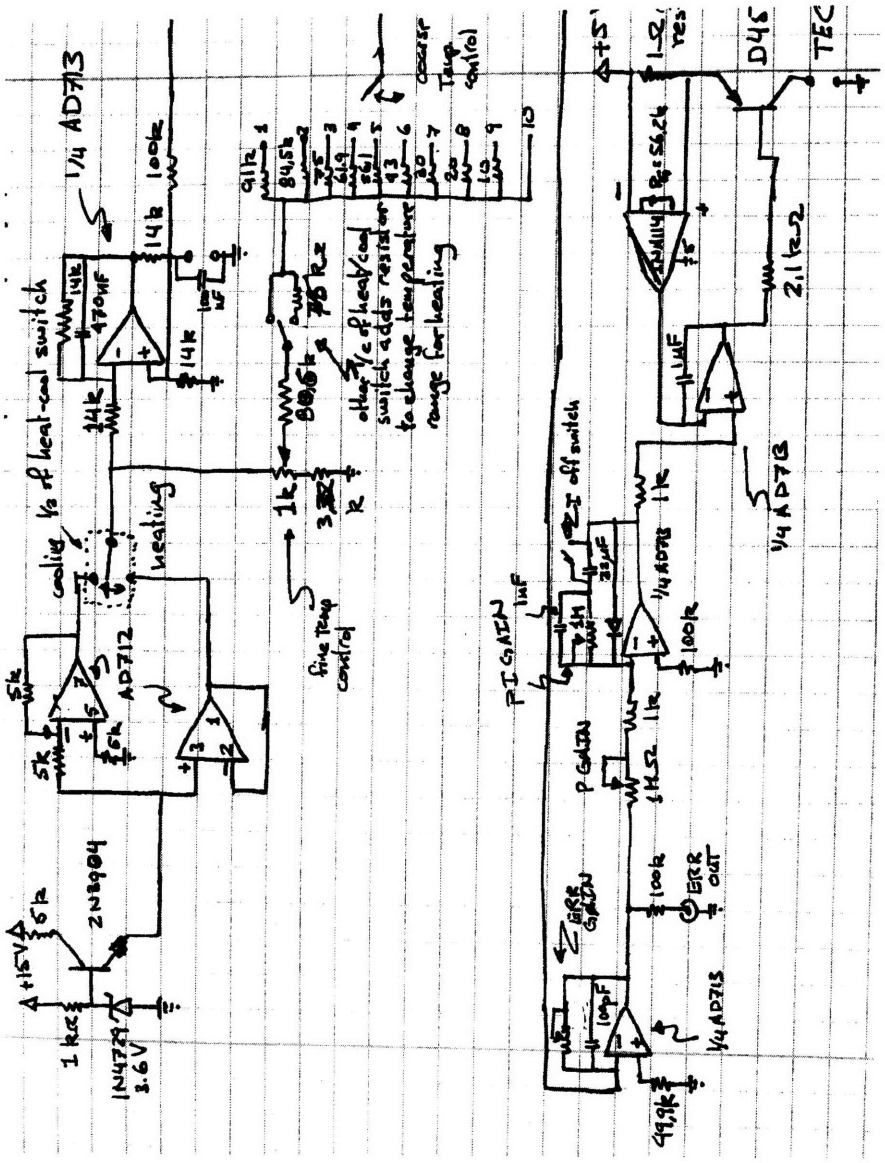

Figure A-1: Circuit diagram of the PI temperature controller.

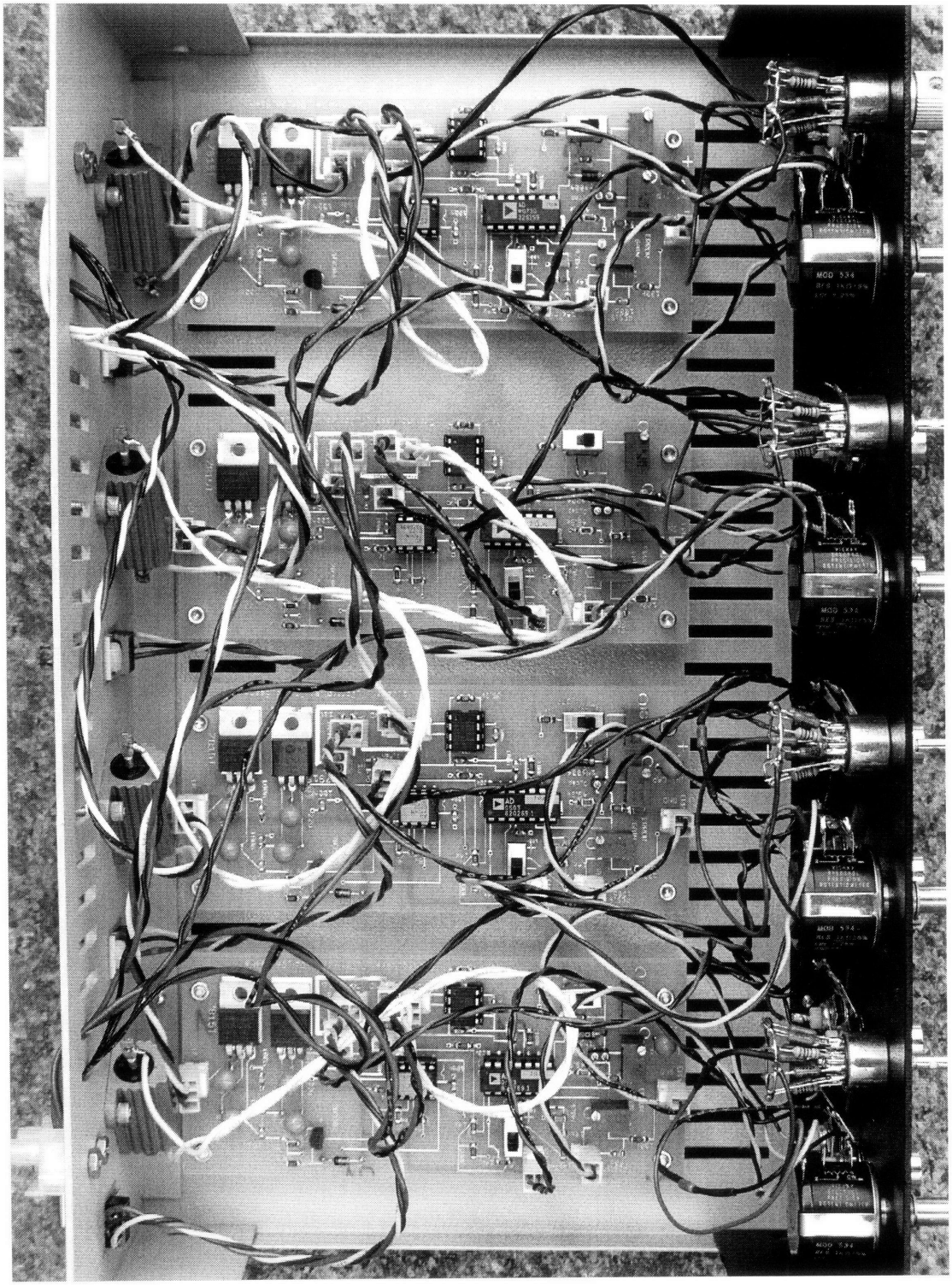

Figure A-2: Completed 4-port PI temperature controller.

Bibliography

[1] A. A. Michelson and E.W. Morley. "On the Relative Motion of the Earth and the Luminiferous Ether." *American Journal of Science.* Vol. XXIV, No 203. (1887).

[2] J. M. Geremia, J. K. Stockton, H. Mabuchi. "Real-Time Quantum Feedback Control of Atomic Spin-Squeezing." *Science.* pp270-273. Vol 304. (2004).

[3] Griffiths, David J. "Introduction to Quantum Mechanics." pp 165. Pearson Education, Inc (2005).

[4] M. Kitagawa and M. Ueda. "Squeezed spin states." *Physical Review A.* 47,5138. (1993).

[5] "Acousto-optic modulators." *Encyclopedia of Laser Physics* [online].

[6] Metcalf, Harold J. and Straten, Peter van der. "Laser Cooling and Trapping." Springer-Verlag New York, Inc. (1999).

[7] E. L. Raab et al. "Trapping of Neutral Sodium Atoms with Radiation Pressure." *Physical Review Letters.* Vol 59, No 23. (1987).

[8] R. H. Dicke. "The Effect of Collisions upon the Doppler Width of Spectral Lines." *Physical Review.* Vol 89, No 2. (1953).

[9] *Atomic Frequency Standards.* Ch. 3.

[10] V. Vuletic, A.J. Kerman, C. Chin, and S. Chu. "Laser Cooling: Beyond Optical Molasses and Beyond Closed Transitions." published in Proceedings of the XVII. International Conference on Atomic Physics (ICAP 2000, Florence), edited by E.

Arimondo, P. De Natale, and M. Inguscio, pp. 356-366, (American Institute of Physics, Melville, New York 2001), invited presentation.

[11] "Magnetic Trap." *wikipedia.com* [online].

[12] "Quantum Manipulation of Ultracold Atoms." *RLE Progress Report.* No. 147, Chapter 16. (2004-2005).

[13] Y. Lin et al. "Impact of the Casimir-Polder Potential and Johnson Noise on Bose-Einstein Condensate Stability Near Surfaces." *Physical Review Letters.* Vol 92, No 5. (2004).

[14] V. Vuletic et al. "Microscopic Magnetic Quadrupole Trap for Neutral Atoms with Extreme Adiabatic Compression." *Physical Review Letters.* Vol 80, No 8. 1998.

[15] "Cooling neutral atoms in a magnetic trap for precision spectroscopy." *Physical Review Letters.* 51, 1336. (1983).

[16] V. Vuletic et al. "Degenerate Raman Sideband Cooling of Trapped Cesium Atoms at Very High Atomic Densities." *Physical Review Letters.* Vol 81, No 26. (1998).

[17] Ketterle, Wolfgang. "The Two-State System: Resonance." *8.421 Lecture Notes.* http://cua.mit.edu/8.421%5FS06/Chapter1.pdf [online] (2006).

[18] P. Treutlein et al. "Coherence in Microchip Traps." *Physical Review Letters.* Vol 92, No 20. (2004).

[19] D. M. Harber et al. "Effect of cold collisions on spin coherence and resonance shifts in a magnetically trapped ultracold gas." *Physical Review A.* 66, 053616. (2002).

[20] V. Vuletic, J. K. Thompson, A. T. Black. "Breaking the Standard Quantum Limit for Atomic Clocks and Generating Single Photons using Optical Cavities and Magnetic Microtraps." *Proposal to DARPA.* (2004).

[21] P. J. Windpassinger et al. "Non-Destructive Probing of Rabi Oscillations on the Cesium Clock Transition near the Standard Quantum Limit." *Physical Review Letters.* 100, 103601. (2008).

[22] "PID Controller." http://www.engin.umich.edu/group/ctm/PID/PID.html (online).

[23] A. Kerman et al. "Beyond Optical Molasses: 3D Raman Sideband Cooling of Atomic Cesium to High Phase-Space Density." *Physical Review Letters.* Vol 84, No 3. (2000).

[24] A. Kuzmich, N. Bigelow, L. Mandel. "Atomic quantum non-demolition measurements and squeezing." *Europhysics Letters.* 42 (5). (1998).

[25] "Quantum projection noise: Population fluctuations in two-level systems." *Physical Review A.* Vol 47, No 5. (1993).

[26] C. Monroe et al. "Very Cold Trapped Atoms in a Vapor Cell." *Physical Review Letters* Vol 65, No 13. (1990).

[27] S. Knappe et al. "A microfabricated atomic clock." *Applied Physics Letters.* Vol 85, No 9. (2004).

[28] V. Vuletic, A.J. Kerman, C. Chin, and S. Chu. "Raman Sideband Cooling in an Optical Lattice." published in Proceedings of the 14th International Conference on Laser Spectroscopy (ICOLS 1999, Innsbruck), edited by R. Blatt, J. Eschner, D. Leibfried, and F. Schmidt-Kaler, pp. 207-216, (World Scientific, Singapore, 1999), invited presentation.

[29] D. J. Wineland et al. "Squeezed atomic states and projection noise in spectroscopy." *Physical Review A.* Vol 50, No 1. (1994).